Statistics of Topological Defects and Spatiotemporal Chaos in a Reaction-Diffusion System

M. Hildebrand, M. Bär,* and M. Eiswirth
Fritz-Haber-Institut der Max-Planck-Gesellschaft, Faradayweg 4-6, D-14195 Berlin, Germany
(Received 27 February 1995)

The transition between rotating spirals and spatiotemporal chaos ("spiral turbulence") in an excitable reaction-diffusion system is investigated by means of statistics of topological defects of the concentration field. The ratio of the variance and the mean value of the number of defects show a significant deviation from unity at this point. A change of the defect dynamics within the turbulent regime reveals a strong similarity to a liquid-to-gas transition, while a liquid-solid-like transition occurs upon a jumplike return to the region of spiral stability.

PACS numbers: 05.45.+b, 05.70.Ln, 82.65.Jv

A variety of recent experimental and theoretical studies revealed complex spatiotemporal dynamics in extended systems [1–8] suggesting an analysis concentrating on objects ("particles"), whose sphere of influence corresponds to a characteristic length scale of the system. Thus the correlation length (from the two-point correlation function of the dynamic variables) has been used as a measure of the extent of spatial coherence in a chaotic pattern [9]. This quantity was shown to illustrate the transition from spiral defect chaos to straight rills in large aspect ratio Rayleigh-Bénard convection [2], as well as the onset of defect-mediated turbulence in nonlinear optical systems [3]. In these systems, the correlation length is equal to the system length in the nonchaotic phase and, therefore, shows a characteristic increase at the transition from the chaotic to the nonchaotic state. In both cases, the objects defining the coherence length were rotating spirals (topological defects) of the phase field. However, for other experiments, especially chemical reaction-diffusion systems with excitable properties [4,5,10], a systematic exploration of the transition between regular patterns like the ubiquitious spiral waves and these presumably chaotic structures has not yet been achieved. In addition, despite a wealth of numerical observations of disordered states in related model systems [1,6–8], there is a lack of systematic understanding of the internal structure of such states. In all these systems, spirals already exist in the nonchaotic, periodic case; their number is constant, depending on the initial conditions, so that there is no unique correlation length for fixed parameters. The chaotic state is characterized by the spontaneous breakup of spirals, which leads to the creation of new spiral pairs [11]. Thus, the characteristic feature of the turbulent state is a nonconstant number of spirals or topological defects.

This observation suggests, in general, a treatment based on the statistics of topological defects, as done previously within the region of defect-mediated turbulence in the complex Ginzburg-Landau equation (CGLE) [1,12]. There the rate of change of the defect number $n(t)$ was assumed to be $\dot{n} = \gamma - \beta n^2$, where γ is the production rate of defects and βn^2 the rate of mutual annihilation. Both β and γ were assumed to be constant in space and time. With these simplifying assumptions, Gil, Lega, and Meunier [12] derived in a simple probabilistic model the equality of the mean number $\overline{n}$ and the variance σ^2 of $n(t)$. This relation has been confirmed in numerical simulations [12,13]. The aim of the present paper is to show that this is not valid in general, because the movement and spatial interaction of the defects play an important role for the overall dynamics. The results will be exemplified with numerical simulations of an excitable medium with a transition to turbulence due to spiral breakup [11].

A generic excitable medium [14] of the FitzHugh-Nagumo type is given by

$$\partial_t u = -\tfrac{1}{\varepsilon}\, u(u-1)\left(u - \frac{v+b}{a}\right) + \Delta u\,, \tag{1a}$$

$$\partial_t v = f(u) - v\,. \tag{1b}$$

With the standard choice $f(u) = u$, Eqs. (1) and related models exhibit only stable spirals. Therefore, we use a modified form corresponding to a delay in the inhibitor production, which is known to possess a transition to spatiotemporal chaos at sufficiently large ε [11]:

$$f(u) = \begin{cases} 0, & u < 1/3 \\ 1 - 6.75u(u-1)^2, & 1/3 \le u \le 1\,, \\ 1, & u > 1\,. \end{cases} \tag{1c}$$

The decisive parameters are b (which is positive for an excitable medium and determines the excitation threshold) and ε (which is the ratio of the time scales of the fast activator and the slow inhibitor variable). For $b > 0$, the reaction part always possesses one stable fixed point ($u = 0$, $v = 0$) and two additional unstable ones. Equations (1) actually represent a reduced version of a realistic surface reaction model, in which the activator variable u corresponds to an adsorbate coverage, while the inhibitor variable v describes a structural surface change [15].

The spatiotemporal dynamics in a representative cut through parameter space with fixed a and b (0.84 and 0.07, respectively) while varying ε is as follows. In the range $0.01 < \varepsilon < 0.06$, suitable initial conditions lead to

the generation of steadily rotating spirals, whose number depends on the initial values of u and v but assumes a constant value after the decay of transients. At $\varepsilon = 0.06$, the spirals undergo a transition from steady rotation to meandering and for $\varepsilon > \varepsilon_c = 0.07$ they break up after some transient rotations, because their smallest rotation period falls below the minimum period allowed by the dispersion relation [11]. At even higher ε the reaction part of Eqs. (1) undergoes a saddle-loop bifurcation ($\varepsilon_{\mathrm{sl}} = 0.19$) which creates a stable limit cycle, but no abrupt changes of the spatiotemporal pattern occur at this point. With further increase of ε this limit cycle vanishes in a Hopf bifurcation ($\varepsilon_{\mathrm{Hopf}} = 0.2245$) and chemical turbulence ceases to exist. Typical snapshots of the spatial distribution of the inhibitor concentration are shown in Fig. 1. Near ε_c the pattern is characterized by spiral segments [Fig. 1(a)]; with increasing ε these segments lose their structure [Fig. 1(c)] until finally a smeared distribution is observed [Fig. 1(d)].

A topological defect is a local zero of the order parameter (see Ref. [1]), which corresponds here to the unstable fixed point in the reaction part of Eqs. (1), given by the equations

$$f(u_0) - v_0 = 0, \qquad \tfrac{1}{3} < u_0 = (v_0 + b)/a < 1. \tag{2}$$

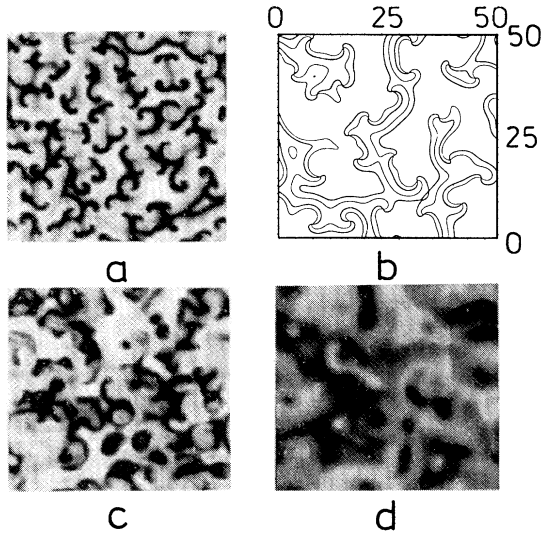

FIG. 1. Typical snapshots of the spatial distribution of the inhibitor concentration [v in Eqs. (1)] for $a = 0.84$ and $b = 0.07$, shown for $\varepsilon = 0.071$ (a), $\varepsilon = 0.125$ (c), and $\varepsilon = 0.2$ (d), after sufficient transient time. The system size is 100×100 spatial units; the simulation was carried out with periodic boundary conditions, and the gray level is proportional to the v concentration. (b) Shows the isoconcentration contours $u = 0.66$ (thicklines) and $v = 0.484$ (thin lines) for the 50×50 section in the upper left corner of the snapshot in (a), which were used for the determination of topological defects as intersections of the two lines.

The locations and number $n(t)$ of topological defects can be obtained numerically from the intersection of the concentration contours u_0 and v_0 [see Fig. 1(b)]. Since below ε_c the tips of the spirals represent just such defects, their study appears as a natural way to characterize the spatiotemporally chaotic state and the accompanying instability. For $\varepsilon < \varepsilon_c$, the value of $n(t)$ reaches a constant number depending on the choice of the initial conditions. In the turbulent regime, $n(t)$ fluctuates around a constant mean value $\overline{n}$ with variance σ^2 after a transient. Both quantities do not depend on the initial conditions. Simulations for different system sizes revealed that $\overline{n}$ and σ^2 are extensive quantities (systematic investigations were carried out in systems with 50–100 defects; the results were checked at selected ε values with up to 1000 defects). Thus the ratio $\sigma^2/\overline{n}$ provides a size-independent measure of the state of the system.

The dependence of σ^2 and $\overline{n}$ on ε is shown in Fig. 2. The transitions to turbulence can be distinguished with the help of the ratio $\sigma^2/\overline{n}$. Approaching the spiral instability it tends to zero, while towards the Hopf bifurcation it approaches unity in accordance with the prediction given in [12]. The value of $\sigma^2/\overline{n}$ can be related directly to the spatial distribution of defects by applying the compressibility equation from hydrodynamics [16], which was introduced in the context of nonequilibrium media in [17]:

$$\frac{\sigma^2}{\overline{n}} = 1 + \frac{\overline{n}}{\Omega^2} \int_{(\mathbf{r}-\mathbf{r}')\in\Omega} \int h(\mathbf{r} - \mathbf{r}')d^2r\, d^2r'. \tag{3}$$

Here Ω is the total area in which defects are counted, $\mathbf{r}$ and $\mathbf{r}'$ are two-dimensional vectors, and $h(\mathbf{r} - \mathbf{r}')$ is the normalized pair correlation function for the defects, defined as

$$h(\mathbf{r} - \mathbf{r}') = \frac{\langle n(\mathbf{r}, t)n(\mathbf{r}', t)\rangle_t}{\langle n\rangle_t^2} - 1. \tag{4}$$

Because of the isotropy of Eqs. (1), $h(\mathbf{r} - \mathbf{r}')$ is also isotropic, i.e., a function of the defect distance $r = |\mathbf{r} - \mathbf{r}'|$ only. Thus $h(r)$ is determined from the probability of finding a second defect at distances between r and $r + dr$ from a given defect. This probability is given by $2\pi r[h(r) + 1]dr/\Omega$. Equations (3) and (4) are a generalization of the concept of Gil, Lega, and Meunier [12], taking into account the influence of spatial correlation between defects on the defect statistics.

In order to illustrate the relations (3) and (4) for our example, we have calculated the pair correlation functions for different values of ε. Right after the breakup transition, $h(r)$ exhibits a "hard core" [Fig. 3(a)] which roughly extends over the range of a correlation length of u. Upon increase of ε, the strong anticorrelation between defects vanishes [Fig. 3(b)], accompanied by a

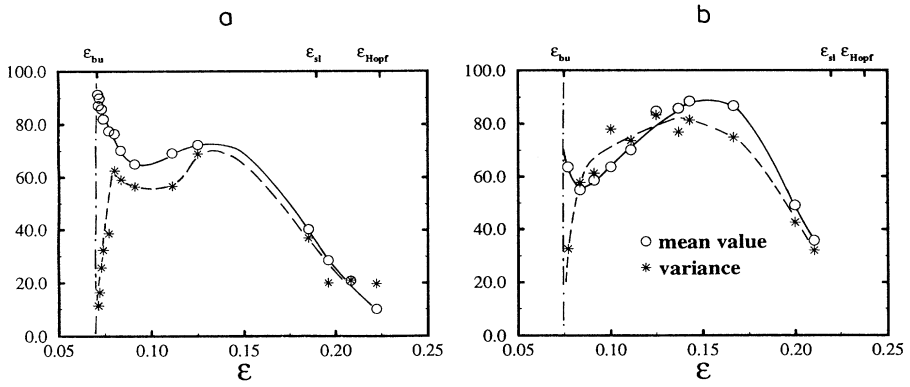

FIG. 2. Dependence of variance σ^2 and mean value $\overline{n}$ of the number of topological defects $n(t)$ on ε for $a = 0.84$ and $b = 0.07$ (a) and $b = 0.14$ (b) in the turbulent regime, averaged over 3000 time units. ε_{bu}, ε_{sl}, and ε_{Hopf} denote the corresponding ε values of the two-dimensional breakup instability and the saddle-loop and Hopf bifurcations in the reaction part of Eqs. (1), respectively.

higher generation rate of defects (and hence decreasing lifetimes). We also observed that defects are now generated closer to an already existing one. These effects are linked to a secondary instability described earlier ("backfiring", cf. Ref. [11]). The corresponding change in the individual trajectories of defects is visualized in Figs. 3(c) and 3(d). Close to the breakup instability, one observes meanderlike paths of a localized nature; i.e., the rotational modes dominate [Fig. 3(c)]. As the generation rate of defects increases, this rotational motion disappears gradually, until eventually the motion is governed almost entirely by translatory, diffusive modes [Fig. 3(d)]. The loss of rotational components of the dynamics and of the hard disk properties of defects is analogous to a liquid-gas transition, more precisely a transformation from a "hard-disk liquid" to a "point gas."

The picture can be extended by looking at the relaxation of turbulent initial conditions after a sudden parameter drop in ε. If the parameter is suddenly shifted to a value of $\varepsilon < \varepsilon_c$, close to the breakup instability, a few spirals fill large parts of the system. These spirals coexist with pointlike defects [Fig. 4(a)]. Thus, the initially turbulent

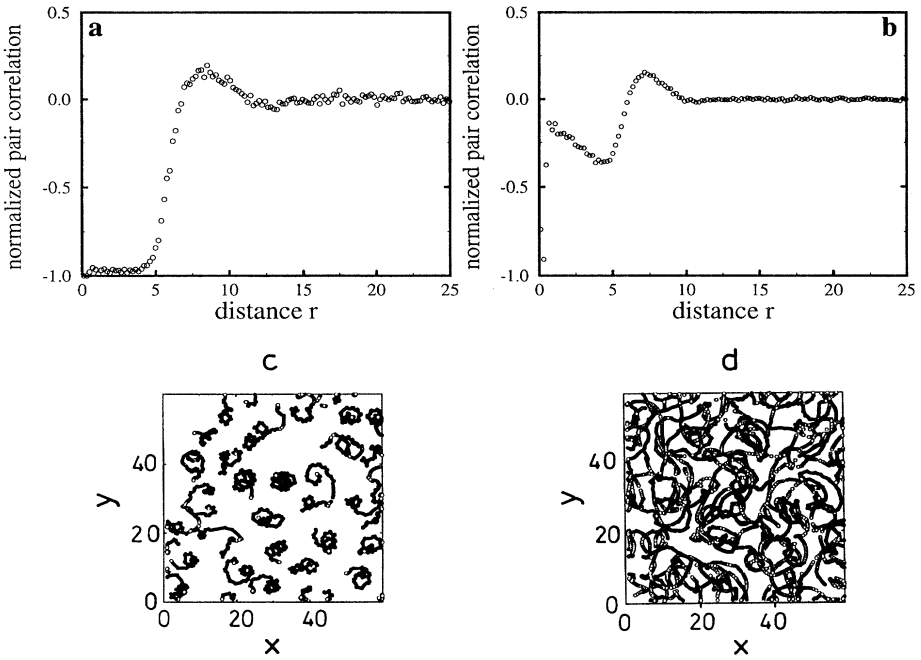

FIG. 3. Normalized pair correlation function $h(r)$ for $a = 0.84$ and $b = 0.07$; $\varepsilon = 0.071$ (a) and $\varepsilon = 0.125$ (b). The system size in the simulation was 200 × 200 spatial units. (c) and (d) show trajectories of topological defects over a period of 77 temporal units in a section of 59 × 59 spatial units for the same system as (a) and (b), respectively.

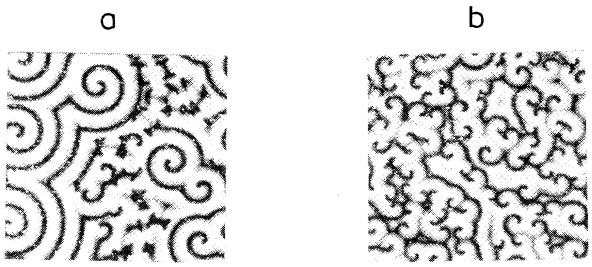

FIG. 4. Snapshots of relaxing turbulent initial conditions [see Fig. 1(a) for $\varepsilon = 0.05$ (a) and $\varepsilon = 0.025$ (b) after 17 000 and 4000 time units, respectively. Note that in (a) the slaved point defects still drift in the field of the nucleated spirals, while in (b) all defects show stable rotation.

concentration distribution slowly relaxes into a (binary) mixture of spirals and point defects. In contrast, a jump to small values of ε well below ε_c transforms all surviving defects of the initial distribution into steadily rotating spirals [Fig. 4(b)]. Because of the purely rotating motion of particles the latter might be called an "amorphous spiral solid." The very slow loss of translatory motion (drift of pointlike defects) in the former case can be associated with the relaxation behavior of a "binary glass." After the breakup, net translatory components of defect motion do not vanish in time anymore, so that, at this point, the picture of a "solid" to "liquid" transition is justified. Related studies in the CGLE focused on the relaxation of random initial conditions [18] and the consequences of the form of interaction on the arrangement of large spiral populations [19].

It should be emphasized that the transition scenario presented above remains valid for large parts of the excitable region ($0 < b < 0.18$). Also in the oscillatory case (small negative b) qualitatively the same behavior has been obtained.

To summarize, we have shown that the statistics of topological defects provides important information about the structure of a spatiotemporally chaotic state. The transition from stable spirals to spiral turbulence here can be regarded as a transition from a "spiral solid" to a "spiral liquid." Inside the turbulent region, a "liquid-gas"-type transition appears in the defect dynamics. Moreover, different transitions to turbulence can be distinguished: While the ratio $\sigma^2/\overline{n}$ of the variance and mean number of defects is unity in the vicinity of a Hopf bifurcation, in accordance with results for the CGLE, this quantity gradually decreases to zero near the spiral-breakup transition. This result may be useful for a general classification of transitions to spatiotemporal chaos. In addition, defect statistics should also be helpful to characterize experimental results on disordered states in related reaction-diffusion systems.

The authors are indebted to A. S. Mikhailov for stimulating discussions and W. Wolf for computational assistance.

*Present address: Department of Chemical Engineering, Princeton University, Princeton, NJ 08544.

[1] P. Coullet, L. Gil, and J. Lega, Physica (Amsterdam) **37D**, 91 (1989).
[2] S. W. Morris, E. Bodenschatz, D. S. Cannell, and G. Ahlers, Phys. Rev. Lett. **71**, 2026 (1993).
[3] F. T. Arrecchi, G. Giacomelli, P. L. Ramazza, and S. Residori, Phys. Rev. Lett. **67**, 3749 (1991).
[4] G. Veser, F. Esch, and R. Imbihl, Catal. Lett. **13**, 371 (1992); G. Ertl, Science **254**, 1750 (1991).
[5] M. Markus, G. Kloss, and I. Kusch, Nature (London) **371**, 402 (1994).
[6] R. V. Sole and J. Valls, Phys. Lett. A **166**, 123 (1992).
[7] A. Hagberg and E. Meron, Phys. Rev. Lett. **72**, 2494 (1994).
[8] A. Karma, Chaos **4**, 461 (1994).
[9] M. C. Cross and P. C. Hohenberg, Science **263**, 1569 (1994).
[10] A. N. Zaikin and A. M. Zhabotinsky, Nature (London) **225**, 535 (1970).
[11] M. Bär and M. Eiswirth, Phys. Rev. E **48**, R1635 (1993); M. Bär, M. Falcke, M. Hildebrand, M. Neufeld, H. Engel, and M. Eiswirth, Chaos **4**, 499 (1994).
[12] L. Gil, J. Lega, and J. L. Meunier, Phys. Rev. A **41**, 1138 (1990).
[13] I. Aranson, L. Kramer, and A. Weber, Phys. Rev. Lett. **72**, 2316 (1994).
[14] D. Barkley, Physica (Amsterdam) **49D**, 61 (1991).
[15] M. Bär, N. Gottschalk, M. Eiswirth, and G. Ertl, J. Chem. Phys. **100**, 1202 (1994).
[16] J. P. Hansen and I. R. McDonald, *Theory of Simple Liquids* (Academic Press, New York, 1976).
[17] A. M. Gutin, A. S. Mikhailov, and V. V. Yashin, Sov. Phys. JETP **65**, 533 (1987).
[18] G. Huber, P. Alstrom, and T. Bohr, Phys. Rev. Lett. **69**, 2380 (1992).
[19] I. S. Aranson, L. Kramer, and A. Weber, Phys. Rev. E **48**, R9 (1993).

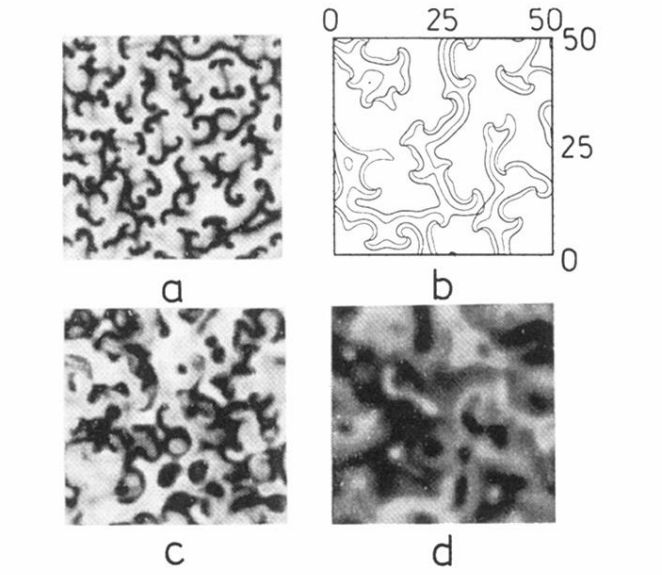

FIG. 1. Typical snapshots of the spatial distribution of the inhibitor concentration [v in Eqs. (1)] for $a = 0.84$ and $b = 0.07$, shown for $\varepsilon = 0.071$ (a), $\varepsilon = 0.125$ (c), and $\varepsilon = 0.2$ (d), after sufficient transient time. The system size is 100×100 spatial units; the simulation was carried out with periodic boundary conditions, and the gray level is proportional to the v concentration. (b) Shows the isoconcentration contours $u = 0.66$ (thicklines) and $v = 0.484$ (thin lines) for the 50×50 section in the upper left corner of the snapshot in (a), which were used for the determination of topological defects as intersections of the two lines.